



# Sulfate formation via aerosol-phase SO<sub>2</sub> oxidation by model biomass burning photosensitizers: 3,4-dimethoxybenzaldehyde, vanillin and syringaldehyde using single-particle mixing-state analysis

Liyuan Zhou<sup>1,2</sup>, Zhancong Liang<sup>1,2</sup>, Brix Raphael Go<sup>1,2</sup>, Rosemarie Ann Infante Cuevas<sup>1,2</sup>,  
Rongzhi Tang<sup>1,2</sup>, Mei Li<sup>3,4</sup>, Chunlei Cheng<sup>3,4</sup>, and Chak K. Chan<sup>1,2,5,a</sup>

<sup>1</sup>School of Energy and Environment, City University of Hong Kong, Hong Kong SAR 999077, China

<sup>2</sup>Shenzhen Research Institute, City University of Hong Kong, Shenzhen 518057, China

<sup>3</sup>Institute of Mass Spectrometry and Atmospheric Environment, Guangdong Provincial Engineering Research Center for On-line Source Apportionment System of Air Pollution, Jinan University, Guangzhou 510632, China

<sup>4</sup>Guangdong–Hong Kong–Macau Joint Laboratory of Collaborative Innovation for Environmental Quality, Guangzhou 510632, China

<sup>5</sup>Low-Carbon and Climate Impact Research Centre of School of Energy and Environment, City University of Hong Kong, Hong Kong SAR 999077, China

<sup>a</sup>current address: Division of Physical Sciences and Engineering, King Abdullah University of Science and Technology, Thuwal, 23955-6900, Saudi Arabia

**Correspondence:** Liyuan Zhou (liyuanzhou3-c@my.cityu.edu.hk) and Chak K. Chan (chak.chan@kaust.edu.sa, chak.k.chan@cityu.edu.hk)

Received: 14 December 2022 – Discussion started: 9 January 2023

Revised: 30 March 2023 – Accepted: 10 April 2023 – Published: 10 May 2023

**Abstract.** Atmospheric oxidation of sulfur dioxide (SO<sub>2</sub>) to sulfate has been widely investigated by means of gas-phase and in-cloud chemistry studies. Recent field measurements have shown significant sulfate formation in cloud-free environments with high aerosol loadings. As an important fraction of biomass burning aerosol components, particulate phenolic and non-phenolic aromatic carbonyls may initiate photosensitized multiphase oxidation of SO<sub>2</sub> in aerosols, of which our knowledge however is still in its nascent stage. In this study, on the basis of single-particle aerosol mass spectrometry (SPAMS) measurements, we find evident sulfate formation in the biomass-burning-derived photosensitizer particles under UV and SO<sub>2</sub> exposure, attributable to photosensitized oxidation of S(IV), while almost no sulfate was observed under dark conditions. The efficiency of sulfate production by photosensitizer particles under UV irradiation, represented by the number percentage of sulfate-containing particles (99 %–43 %) and the relative peak area (RPA) of sulfate (0.67–0.12) in single-particle spectra, in descending order, were 3,4-dimethoxybenzaldehyde (DMB), vanillin (VL) and syringaldehyde (SyrAld). Internal mixtures of VL and potassium nitrate (KNO<sub>3</sub>) gave a slightly lower number percentage and RPA of sulfate than VL particles alone. In externally mixed VL and KNO<sub>3</sub> particles, sulfate was predominantly formed on the former, confirming that sulfate formation via photosensitization prevails over that via nitrate photolysis. Our results suggest that photosensitized oxidation of S(IV) could make an important contribution to aerosol sulfate formation, especially in areas influenced by biomass burning.

## 1 Introduction

Sulfate is a key component of fine particulate matter in the atmosphere, which impacts air quality, climate, and human and ecosystem health (Nel, 2005; Fuzzi et al., 2015; Grantz et al., 2003). Traditional atmospheric models that include the gas-phase oxidation of sulfur dioxide ( $\text{SO}_2$ ) by the hydroxyl radical ( $\cdot\text{OH}$ ) (Calvert et al., 1978) and stabilized Criegee intermediates (Cheng et al., 2016), as well as a series of aqueous, in-cloud oxidation of  $\text{SO}_2$ , underpredict the sulfate production during heavy pollution episodes in China (Zheng et al., 2015; Zhang et al., 2015; Wang et al., 2014; Liu and Abbatt, 2021). Although the liquid water content (LWC) is generally much lower in aerosol particles than in fog and cloud droplets, it was reported that multiphase oxidation processes in aerosol particles are important, especially in polluted and high-relative-humidity (RH) conditions (Liu et al., 2021, 2020). The typical oxidants involved in multiphase oxidation of S(IV) in aerosol particles include dissolved ozone ( $\text{O}_3$ ) (Hoffmann and Calvert, 1985), hydrogen peroxide ( $\text{H}_2\text{O}_2$ ) (Hoffmann and Calvert, 1985), transition metal ions (TMIs; i.e., Fe (III) and Mn(II)) (Ibusuki and Takeuchi, 1987; Harris et al., 2013; Alexander et al., 2009; Martin and Good, 1991), methyl hydrogen peroxide (Walcek and Taylor, 1986) and peroxyacetic acid (Walcek and Taylor, 1986). To narrow the gap between the measured and modeled sulfate production, new chemical pathways have been suggested, involving nitrogen dioxide ( $\text{NO}_2$ ) (Wang et al., 2016; Cheng et al., 2016), organic peroxides (Yao et al., 2019; Ye et al., 2018), oxidants from particulate nitrate photolysis (Gen et al., 2019a, b; Zhang et al., 2020) and hypohalous acid (HOX; e.g., HOCl and HOBr) (Liu and Abbatt, 2020). However, the missing sulfate source has still remained unclear and controversial.

Photosensitization in atmospheric aerosols has been recently proposed to initiate novel chemistry in the formation of secondary pollutants (George et al., 2015). Upon irradiation, atmospheric photosensitizers such as aromatic carbonyls can generate triplet excited states ( $^3\text{C}^*$ ) (Canonica et al., 1995; Anastasio et al., 1996; Smith et al., 2014; Kaur and Anastasio, 2018; Kaur et al., 2019; Smith et al., 2016), which can oxidize phenols at higher rates compared to  $\cdot\text{OH}$ , particularly under acidic conditions (Smith et al., 2014). In addition to being an oxidant,  $^3\text{C}^*$  can also react with  $\text{O}_2$  to generate secondary oxidants, such as singlet oxygen ( $^1\text{O}_2$ ), superoxide ( $\text{O}_2^{\cdot-}$ ), hydroperoxyl radical ( $\cdot\text{HO}_2$ ) and  $\cdot\text{OH}$  (Corral Arroyo et al., 2018; Dalrymple et al., 2010; George et al., 2018). Biomass burning is an important source of aromatic carbonyls (Rogge et al., 1998; Nolte et al., 2001; Schauer et al., 2001), and the concentrations of phenolic and non-phenolic carbonyls are comparable in biomass burning smoke (Simoneit et al., 1993; Anastasio et al., 1996). Direct photosensitized oxidation of vanillin (VL; a typical aromatic carbonyl photosensitizer) has been reported as an important pathway to form aque-

ous secondary organic aerosol (SOA) in areas influenced by biomass burning, with reaction products dominated by brown carbon chromophores (Mabato et al., 2022, 2023). However, only limited studies focused on the role of biomass-burning-derived photosensitizers in S(IV) oxidation. Wang et al. (2020) reported that photosensitized chemistry involving the humic fraction of aerosols during Chinese haze events could explain a significant fraction of the observed sulfate formation, which highlighted the potential photosensitizing properties of biomass burning particles. Naphthalene, emitted primarily from fossil fuel combustion and biomass burning, can be oxidized by OH to form secondary organic aerosol, which was observed to possess interfacial photosensitizing properties (Wang et al., 2021). These recent studies have advanced our understanding of the photosensitized processes, but the types of photosensitizers from biomass burning are diverse and their properties are complex, preventing us from further assessing the importance of photosensitized sulfate formation in the dynamic ambient atmosphere. In this study, we investigate sulfate formation via aerosol-phase  $\text{SO}_2$  oxidation by biomass-burning-derived aromatic carbonyl photosensitizers, including both non-phenolic (3,4-dimethoxybenzaldehyde, DMB) and phenolic photosensitizers (vanillin, VL, and syringaldehyde, SyrAld) with similar molar absorptivity at atmospheric-relevant wavelengths (Fig. S1 in the Supplement), in an oxidation flow reactor (OFR) utilizing a single-particle aerosol mass spectrometer (SPAMS). Similar to photosensitization, nitrate photolysis has been reported as a typical sulfate formation pathway initiated by particulate photoactive compounds (Gen et al., 2022). The objectives of this study are to semi-quantitatively evaluate the extent of sulfate formation in photosensitizer particles and qualitatively compare the relative atmospheric importance of particulate photosensitization and nitrate photolysis in sulfate formation.

## 2 Methods

### 2.1 Materials and experimental setup

A vaporization–condensation method was used to coat photosensitizing or non-photosensitizing species on  $0.3\text{ }\mu\text{m}$  polystyrene latex sphere (PSL) particles (Thermo Fisher Scientific Inc., MA) (Qi et al., 2019). A detailed experimental setup is shown in Fig. S2a, and the initial experimental conditions are summarized in Table S1. All chemicals, including DMB (Acros Organics, 99+ %), VL (Acros Organics, 99 %), SyrAld (Sigma Aldrich, 98 %), benzoic acid (BA; Acros Organics, 99.6 %), potassium nitrate ( $\text{KNO}_3$ ; Sigma Aldrich, 99+ %) and oxalic acid (Sigma Aldrich, 99.9+ %), were used as purchased. The structures of the chemicals used are provided in Table S2. The PSL particles were selected as condensation nuclei due to their chemically and thermally inert nature. Their size did not change upon passing through the dryer or glass bottle in a  $120^\circ\text{C}$  oil bath or exposure

to SO<sub>2</sub> or UV irradiation (Fig. S3). In addition, PSL particles are difficult to be ionized and do not complicate the interpretation of mass spectra. The PSL condensation nuclei were generated by using a constant output atomizer (TSI 3076) with pure N<sub>2</sub> gas (> 99.995 %), and a portion of the particles passed through a diffusion dryer at a flow rate of 300 mL min<sup>-1</sup> to achieve RH < 10 %. The dried particles subsequently passed through a heated glass bottle (inlet about 2 in. (5 cm) above the bottom) containing ~ 0.5 g of either DMB, VL, SyrAld or BA at the bottom. The heating temperatures of the glass bottle were regulated using an oil bath near the melting points of the chemicals. The generated organic vapor condensed to form coatings onto the PSL particles. The coating thickness was estimated by the measured particle size increase by the SPAMS. For control experiments with PSL-only particles, the particles passed through the same glass bottle containing no chemicals. Coated particles of photosensitizing (DMB, VL, SyrAld) (Smith et al., 2015, 2016, 2014) and non-photosensitizing (BA) (Smith et al., 2015) species or uncoated PSL-only particles were then introduced into an OFR (volume of approximately 7.2 L) and mixed with SO<sub>2</sub> gas. The SO<sub>2</sub> was delivered by a flow of around 11 mL min<sup>-1</sup> (203 ppm, mixing with pure N<sub>2</sub>, Scientific Gas Engineering Co., Ltd.) to achieve the SO<sub>2</sub> concentration of around 750 ppb in the OFR. Depending on the experiment, the RH in the OFR was regulated at ~ 80 % or 20 % to achieve different content of aerosol water by passing high-efficiency particulate air-filtered and activated-carbon-denuded compressed air or pure N<sub>2</sub> through water bubblers. Note that the photosensitizers may be (polymorphic) solid or semi-solid due to their low solubility and hygroscopicity, even at 80 % RH (Kavuru et al., 2016; Hussain et al., 2001). For example, Mochida and Kawamura (2004) reported that pyrolysis products of lignin with –COOH, including vanillic acid and syringic acid, showed no hygroscopic growth, even at RH of more than 90 %. They also proposed that other pyrolysis products with chemical structures such as –CHO may have even lower hygroscopicity than –COOH and would not show measurable particle growth. Though we could not observe the phase states of the particles, both aerosol liquid water in (partially) deliquescent particles and surface-adsorbed water content on solid particles at 80 % RH were expected to be higher than at 20 % RH (Rubasinghege and Grassian, 2013). Experiments under air enable the generation of secondary oxidants. Conversely, the N<sub>2</sub> experiments would inhibit the formation of secondary oxidants, which can lead to triplet-driven reactions (Chen et al., 2020). The total flow in the OFR was around 3 L min<sup>-1</sup>, resulting in a residence time of ~ 2.5 min. There are four UVA lamps (Shenzhen Guan hongrui Technology Co., Ltd.) with a continuous emission spectrum over 310–420 nm surrounding the OFR. We conducted experiments with one and four lamps to provide a total irradiance of about  $1.1 \times 10^{15}$  ( $I_1$ ) and  $3.8 \times 10^{15}$  ( $I_4$ ) photon cm<sup>-2</sup> s<sup>-1</sup>, respectively (see details in Sect. S1), and dark control experiments were performed with UV lamps

switched off. Each experiment lasted around 20 min. In the absence of light and SO<sub>2</sub>, there was no change in the mass spectra of coated particles (Fig. S4). At the outlet of the OFR, the SO<sub>2</sub> concentration was monitored by a SO<sub>2</sub> analyzer (Teledyne, T100, USA), and the size and chemical composition of individual aerosol particles were analyzed by a single-particle aerosol mass spectrometer (SPAMS; Hexin Analytical Instrument Co., Ltd, China). This single-particle technique allows us to study the mixing state of the particles. KNO<sub>3</sub> was widely observed in biomass burning plumes (Zauscher et al., 2013). Internally mixed particles of photosensitizing species and KNO<sub>3</sub> were generated by atomizing aqueous solutions of KNO<sub>3</sub> with several drops of PSL suspension, followed by passing through a dryer and then the heated glass bottle containing photosensitizing species as described above (Fig. S2a). Externally mixed particles were generated with a second atomizer (TSI 9032), and the generated KNO<sub>3</sub> or KNO<sub>3</sub>–oxalic acid mixed particles were then mixed with photosensitizing-species-coated particles in a stainless-steel chamber ( $\phi 8 \times 20$  cm) before introduction to the OFR (Fig. S2b).

## 2.2 SPAMS and data analysis

A detailed description of the operational principle of SPAMS has been provided elsewhere (Li et al., 2011). Briefly, aerosol particles were introduced into the SPAMS through an orifice and aerodynamic lens and consecutively irradiated by two laser beams, where their aerodynamic diameter were determined through the velocity and flight time. The sized particles were then desorbed and ionized by a pulsed 266 nm laser (0.5 mJ), which was triggered at the precise time on the basis of the particle velocities. The produced positive and negative molecular fragments were analyzed by a Z-shaped bipolar time-of-flight mass spectrometer (Pratt et al., 2009; Li et al., 2011). The ionization efficiency of the SPAMS to detect 250–2000 nm atmospheric aerosol particles was above 30 % on average (Li et al., 2011). The number of ionized particles for each experiment condition was around 1000–3000, sufficient for systematically identifying the heterogeneous reaction products (Liang et al., 2022; Qi et al., 2019). Furthermore, each experiment was repeated, as reflected in Fig. S6. Single-particle size and mass spectral analyses were performed using the Computational Continuation Core (COCO) toolkit based on MATLAB software. The number percentage and relative peak area (RPA; defined as the fractional contribution of the targeted ion peak area to the sum of all ion peak areas) were applied to indicate the variations of the amount of different species (e.g., sulfate) in individual particles (Hu et al., 2022). Sulfate-containing particles were distinguished by  $m/z$  –97 [HSO<sub>4</sub><sup>-</sup>] or  $m/z$  –96 [SO<sub>4</sub><sup>-</sup>] (Guazzotti et al., 2001; Liang et al., 2022). In addition, a neural network algorithm based on an adaptive-resonance-theory-based neural network algorithm (ART-2a) (Li et al., 2011) was used to separate and cluster particles in external and internal mix-

tures according to the similarities in individual mass spectra of single particles. Before entering the SPAMS, the particles passed through a diffusion dryer to reduce the matrix effects from water (Neubauer et al., 1998).

### 3 Results and discussion

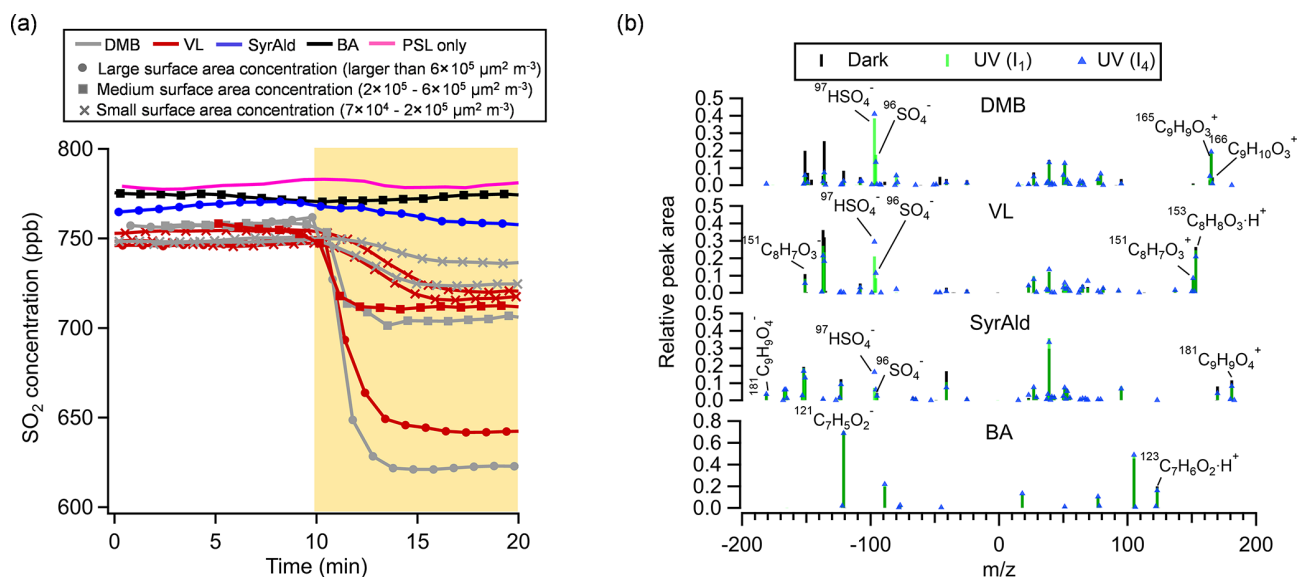
#### 3.1 Photosensitized SO<sub>2</sub> uptake and sulfate formation

Figure 1a shows the changes in SO<sub>2</sub> concentration ([SO<sub>2</sub>]) in the presence of PSL particles coated with various types of photosensitizing (DMB, VL and SyrAld) and non-photosensitizing (BA) species under dark and UV irradiation conditions. In Fig. 1a, under UV conditions, only time traces of SO<sub>2</sub> under *I*<sub>4</sub> UV irradiance were shown for clarity, and cases of *I*<sub>1</sub> UV irradiance can be found in Fig. S5. Unless stated otherwise, results shown in the following discussions were obtained at 80 % RH. The steady concentration of SO<sub>2</sub> in the OFR was at around 750 ppb under dark conditions. Upon exposure to UV light, a rapid drop in the SO<sub>2</sub> concentration was observed in the presence of DMB- and VL-coated particles, indicating photoinduced uptake of SO<sub>2</sub> on these particles. Wang et al. (2021) suggested that the photosensitized chemical reactions between naphthalene-derived SOA and SO<sub>2</sub> likely occur at/near the particle surface. In this study, the SO<sub>2</sub> consumption under UV irradiation conditions for DMB- and VL-coated particles increased with the surface area of SPAMS-detected particles in the OFR (Figs. 1a and S6) ( $R^2 = 0.84\text{--}0.99$ ). Total surface area concentrations of  $7 \times 10^4\text{--}2 \times 10^5 \mu\text{m}^2 \text{m}^{-3}$ ,  $2 \times 10^5\text{--}6 \times 10^5 \mu\text{m}^2 \text{m}^{-3}$ , and larger than  $6 \times 10^5 \mu\text{m}^2 \text{m}^{-3}$  are denoted as “small”, “medium”, and “large”, respectively. These values fall within the urban background and indoor air ranges but are slightly lower than urban pollution ranges (Willeke and Whitby, 1975; Hudda and Fruin, 2016; Qi et al., 2008). The SO<sub>2</sub> consumption per unit surface area concentration also increased with higher UV irradiance (Fig. S6). Only slight SO<sub>2</sub> consumption under UV irradiation conditions was observed in the presence of SyrAld-coated particles, and no observable decrease in SO<sub>2</sub> concentrations was found in the absence of photosensitizing species, i.e., BA-coated particles and PSL-only particles. The average mass spectra of DMB-, VL-, SyrAld- and BA-coated single particles under dark and UV irradiation conditions in the presence of SO<sub>2</sub> are shown in Fig. 1b, characterized by their respective parent ions (in either neutral, protonated or deprotonated form) and expected smaller organic fragment ions. The PSL-only particles do not ionize, and no mass spectra were observed (Qi et al., 2019). No sulfate was formed under dark conditions, consistent with the stable SO<sub>2</sub> concentrations observed. However, upon exposure to UV irradiation, the RPA of sulfate ( $^{97}\text{HSO}_4^-$  and  $^{96}\text{SO}_4^-$ ) increased significantly, accompanied by the slight decrease of RPA of the parent ions of  $^{165}\text{C}_9\text{H}_9\text{O}_3^{+/-}$ ,  $^{153}\text{C}_8\text{H}_9\text{O}_3^{+/-}$  and  $^{181}\text{C}_9\text{H}_9\text{O}_4^{+/-}$  for DMB-, VL- and SyrAld-coated particles, respectively. Mabato et

al. (2022) reported direct photosensitized oxidation of photosensitizers, which can generate oxygenated products such as functionalized monomers and oxygenated ring-opening products. In this study, we observed the peak of  $^{181}\text{C}_9\text{H}_9\text{O}_4^+$  (DMB + O) upon UV irradiation, but the identification of organic products was generally limited by laser-induced fragmentation in the SPAMS. Although the coating thickness estimated by particle size increase spanned a wide range from 100 nm to 2.2  $\mu\text{m}$ , the number percentage and RPA of sulfate generally exhibited the same trend for the studied photosensitizers in each size bin (Fig. S7). Figure 2 shows the average RPA of sulfate (circles) and the number percentage of sulfate-containing particles (diamonds) in DMB-, VL-, SyrAld- and BA-coated particles under dark conditions and at different UV intensities in the presence of SO<sub>2</sub> with the corresponding SO<sub>2</sub> consumption normalized by the average total particle surface area concentration before and after UV irradiation in the OFR detected by SPAMS (crosses). The RPA and number percentage of sulfate for each experimental condition were calculated by taking the average of those values in different size bins in Fig. S7. Hence the potential uneven coating thickness has been incorporated in the averages, which show consistent trends in Fig. 2. The average number percentages of sulfate-containing particles in DMB- and VL-coated particles are considerably higher (> 84 %) under both *I*<sub>1</sub> and *I*<sub>4</sub> UV irradiances than under dark (< 2 %) conditions. The SyrAld-coated particles gave a slightly lower percentage of sulfate-containing particles of 43 % and 83 % at *I*<sub>1</sub> and *I*<sub>4</sub> UV irradiances, respectively. Upon increase of photon flux densities (*I*<sub>1</sub> to *I*<sub>4</sub>), the RPA of sulfate increases for DMB-, VL- and SyrAld-coated particles, which is in line with the enhanced normalized SO<sub>2</sub> consumptions. The number percentage and RPA of sulfate exhibited a similar descending order of DMB > VL > SyrAld > BA in each size bin (Fig. S7). The pHs of the DMB ( $6.01 \pm 0.06$ ), VL ( $6.15 \pm 0.12$ ) and SyrAld ( $5.97 \pm 0.10$ ) particles were similar. Our observed trend of sulfate formation potential is in line with the secondary organic aerosol mass yield for syringol oxidation by  $^3\text{C}^*$  of DMB (114 %), VL (111 %) and SyrAld (78 %) in the literature (Smith et al., 2016, 2014). Specifically, DMB has a higher quantum yield and longer lifetime of  $^3\text{C}^*$  compared to VL (Felber et al., 2021), which can result in a higher sulfate formation efficiency. On the other hand, the direct photodegradation rate constant was higher for SyrAld than VL, likely suppressing the concentration of SyrAld in droplets/particles and the photosensitized oxidation (Smith et al., 2016). Photosensitization in atmospheric chemistry is still a research field with broad uncertainties (Felber et al., 2021). Further quantitative work on the quantum yield, the lifetime, and the decay and quenching rate constants of the  $^3\text{C}^*$  is needed.

The loss of SO<sub>2</sub> associated with the synchronous sulfate production in single DMB-, VL-, and to a lesser extent, SyrAld-coated particles was likely attributed to the photosensitization-induced oxidation of S(IV) (i.e., SO<sub>2</sub>,





**Figure 1.** (a) Time traces of  $\text{SO}_2$  in the dark (0–10 min) and under UV irradiation ( $I_4$ ) (10–20 min) in the presence of DMB-, VL-, SyrAld-, or BA-coated particles and PSL-only particles. The  $\text{SO}_2$  consumption is presented as a function of the total surface area concentration of SPAMS-detected particles. Total surface area concentrations of  $7 \times 10^4$ – $2 \times 10^5 \mu\text{m}^2 \text{m}^{-3}$ ,  $2 \times 10^5$ – $6 \times 10^5 \mu\text{m}^2 \text{m}^{-3}$ , and larger than  $6 \times 10^5 \mu\text{m}^2 \text{m}^{-3}$  are denoted as “small”, “medium”, and “large”, respectively. (b) Average negative and positive mass spectra for the DMB-, VL-, SyrAld- and BA-coated particles under dark and UV irradiation ( $I_1$  and  $I_4$ ) conditions in the presence of  $\text{SO}_2$ . All experiments were conducted at 80 % RH.

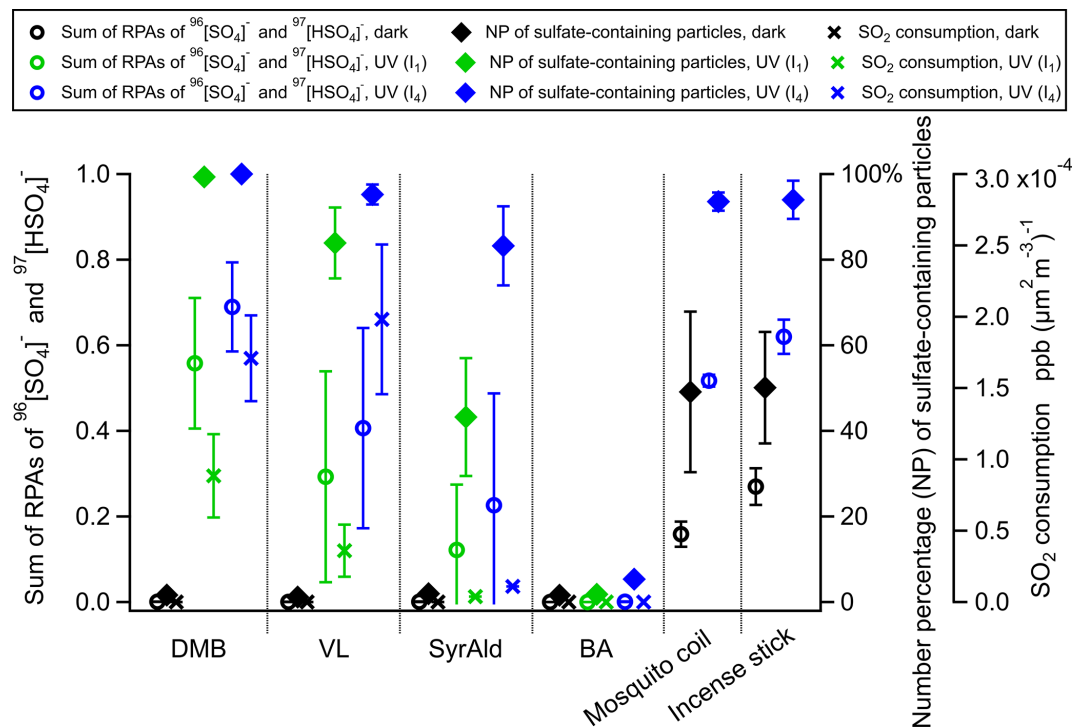


**Figure 2.** Average sulfate relative peak area (RPA) and number percentage (NP) of sulfate-containing particles for the DMB-, VL-, SyrAld- and BA-coated particles, mosquito coil burning particles and incense burning particles under dark and UV irradiation conditions in the presence of  $\text{SO}_2$ . Errors are shown by 95 % confidence intervals. The  $\text{SO}_2$  consumptions normalized by the average total particle surface area concentrations before and after UV irradiation in the OFR detected by SPAMS are shown. Data of incense and mosquito coil burning particles are from Liang et al. (2022). All experiments were conducted at 80 % RH.

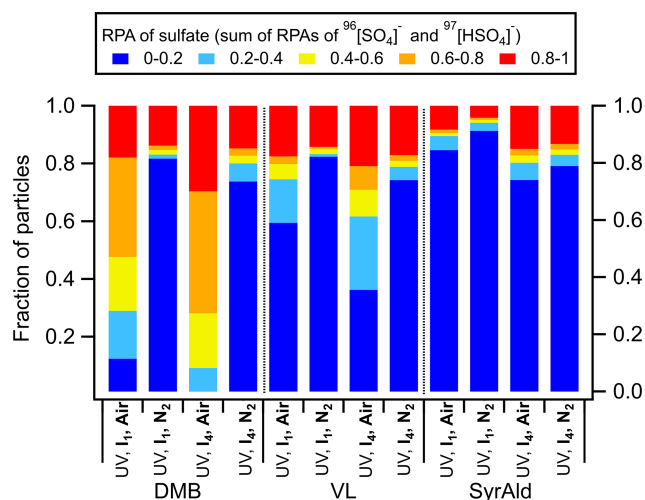


**Figure 3.** Distribution of sulfate RPA for DMB-, VL- and SyrAld-coated particles under air and N<sub>2</sub> conditions at different UV intensities in the presence of SO<sub>2</sub>.

HSO<sub>3</sub><sup>−</sup> and SO<sub>3</sub><sup>2−</sup>). Specifically, UV irradiation could excite photosensitizers from their ground state to singlet excited state, then rapidly relax to a triplet state via intersystem crossing (George et al., 2015; Gomez Alvarez et al., 2012). The S(IV) could be oxidized to sulfate directly by <sup>3</sup>C\* or by the secondary oxidants (e.g., <sup>1</sup>O<sub>2</sub>, O<sub>2</sub><sup>•−</sup>/<sup>•</sup>HO<sub>2</sub> and <sup>•</sup>OH) produced from the excited molecules and O<sub>2</sub>. Wang et al. (2020) observed sulfate production from direct reactions between triplets of 4-(benzoyl) benzoic acid, humic acid and their salts, and hydrated S(IV).

In our previous study, we have reported the enhanced SO<sub>2</sub> oxidation and sulfate formation in incense and mosquito coil burning particles (Liang et al., 2022), as surrogates of biomass burning organic aerosol (BBOA; Li et al., 2012; Zhang et al., 2014), under light, when compared with dark conditions. The number percentage of sulfate-containing particles increased from around 50 % under dark conditions to around 90 % after UV irradiation (Fig. 2). Incense burning particles contain a variety of photosensitizers, e.g., DMB, VL and SyrAld (Peng et al., 2020; Liu and Sun, 1988; Liang et al., 2022), which could oxidize SO<sub>2</sub> via photosensitization. In contrast to Liang et al. (2022), we did not observe sulfate formation under dark conditions in the current study. Their much higher percentage of sulfate-containing particles under dark conditions was likely due to the gaseous oxidants in incense burning plumes in their experiments. Furthermore, as mentioned earlier, in the control experiment using BA-coated particles as seeds in the presence of SO<sub>2</sub>, neither the RPA of sulfate nor the number percentage of sulfate-containing particles changed upon irradiation. This indicates that the direct photoexcitation of SO<sub>2</sub> in the presence of water to form <sup>•</sup>OH and subsequently sulfate plays a negligible role (Kroll et al., 2018; Martins-Costa et al., 2018; Wang et al., 2021).

### 3.2 The potential role of secondary oxidants

The triplet excited state (<sup>3</sup>C\*) of aromatic carbonyls can react with O<sub>2</sub> in air-saturated conditions via either energy transfer to form <sup>1</sup>O<sub>2</sub> or electron transfer to form O<sub>2</sub><sup>•−</sup>, which can further react with H<sup>+</sup> ion to produce H<sub>2</sub>O<sub>2</sub> and <sup>•</sup>OH (Dalrymple et al., 2010). Therefore, the absence of O<sub>2</sub> in N<sub>2</sub>-saturated experiments would inhibit the formation of secondary oxidants. Figure 3 shows that replacing air by pure N<sub>2</sub> substantially shifted the distribution of RPAs for DMB- and VL-coated particles toward the lower end, while SyrAld-coated particles exhibited slight changes. For example, DMB-coated particles with sulfate RPA larger than 0.6 were dominant and comprised more than 52 % of total particles in air, but sulfate RPA of 0–0.2 accounts for more than 73 % of the total particles in N<sub>2</sub> under both UV irradiances. This suggests the involvement of O<sub>2</sub> and the potentially important role of secondary oxidants in sulfate formation. Upon the increase of UV intensity (from I<sub>1</sub> to I<sub>4</sub>), the number fraction of particles with sulfate RPA larger than 0.2 only slightly increased in N<sub>2</sub>-saturated conditions, and particles with RPA of 0–0.2 dominated the population, indicating the lower ability of direct <sup>3</sup>C\* oxidation of SO<sub>2</sub> to produce a large sulfate RPA. The relative importance of the direct <sup>3</sup>C\* and secondary oxidants in sulfate production varies among the different compounds, as reflected by the distribution of sulfate RPAs in Fig. 3. For example, secondary oxidants could be more important in the DMB system than the SyrAld system. In contrast, Wang et al. (2020) reported that switching from air to N<sub>2</sub> resulted in similar S(IV) oxidation rates, indicating that the direct reaction of SO<sub>2</sub> with <sup>3</sup>C\* was more significant than that with the secondary oxidants for 4-(benzoyl)benzoic acid. This discrepancy is possibly due to the different reactivities of <sup>3</sup>C\* from different photosensitizing chemicals towards SO<sub>2</sub> (Wang et al., 2020). In air, DMB-coated particles exhibited the strongest SO<sub>2</sub> oxidation potential with 88 % of the total particles having sulfate RPAs larger than 0.2 (I<sub>1</sub>), followed by VL-coated (41 %) and SyrAld-coated (15 %) particles. Upon exposure to simulated sunlight, SyrAld and VL have been shown to undergo apparent direct photodegradation, but DMB exhibits smaller or almost no loss in illuminated solution mixed with non-carbonyl phenols or benzenediols (Smith et al., 2016, 2015, 2014; Mabato et al., 2023, 2022). This is generally consistent with the decrease of RPAs of parent ions in this study (Fig. S8). The rapid direct photodegradation of phenolic carbonyls (VL and SyrAld) can reduce their concentrations in the particles and limits the formation of sulfate.

### 3.3 Relative importance of particulate photosensitization and nitrate photolysis in sulfate formation

Nitrate is a ubiquitous constituent of atmospheric aerosol particles (Chan and Yao, 2008). Multiphase photochemical oxidation of  $\text{SO}_2$  by the photolysis of particulate nitrate could make an important contribution to aerosol sulfate formation (Gen et al., 2019a, b). To qualitatively compare the relative atmospheric importance of photosensitization and nitrate photolysis in sulfate formation, external mixtures of VL-coated particles and  $\text{KNO}_3$  particles were exposed to  $\text{SO}_2$  and UV irradiation at 80 % RH. Vanillin was used for comparison owing to its moderate sulfate formation potential among the three photosensitizers tested. Potassium was the dominant cation in biomass burning plumes (Jahn et al., 2021; Frenay et al., 2009; Zhang et al., 2022), and therefore,  $\text{KNO}_3$  was selected as the model nitrate salt. The RPA of sulfate for VL-coated particles and  $\text{KNO}_3$  particles at different sizes in the external mixture was compared in Fig. 4a. The VL-coated particles exhibited an average sulfate RPA of 0.26, with an overall inverse relationship with particle size, while the absolute peak areas (APAs) of sulfate are moderately higher for large particles. The APA is proportional to the absolute number of ions detected, and a larger sulfate APA may indicate a larger amount of sulfate formed. However, APAs are more sensitive to the variability in ion intensities associated with particle–laser interactions than RPAs (Gross et al., 2000; Hatch et al., 2014; Zhou et al., 2022). The variation in RPAs was smaller than that in APAs, even though some studies found that the RPA values may also be affected by the inherent variability of particle compositions due to matrix effects within particles (Reinard and Johnston, 2008; Zhou et al., 2016). The reactive uptake comprises the diffusion of  $\text{SO}_2$  molecules, followed by oxidation of  $\text{SO}_2$  at/near the surface or in the bulk of the particles. The decreased sulfate RPA with increasing particle size suggested the photosensitized sulfate formation at/near the surface of VL-coated particles, probably due to the prevalence of surface reactions or diffusional limitations of  $\text{SO}_2$  in larger particles, especially in the poorly hygroscopic and potentially viscous VL matrix. We cannot exclude the occurrence of bulk-phase reaction in the organic moiety, though it was likely less efficient than the surface reaction. In contrast, deliquescent  $\text{KNO}_3$  particles (Fig. S9) exhibited RPAs of 0, suggesting that nitrate photolysis plays a negligible role in our study, although the concentration of  $[\text{NO}_3^-]$  in  $\text{KNO}_3$  particles at 80 % RH was estimated to be 6.3 M by AIOMFAC (<http://www.aiomfac.caltech.edu>, last access: 10 October 2022) (Zuend et al., 2008), almost 100 times higher than the solubility of VL ( $\sim 66$  mM). At 80 % RH, the pH of  $\text{KNO}_3$  particles was  $6.38 \pm 0.07$  comparable to that of VL ( $\text{pH} = 6.15 \pm 0.12$ ). Thus, pH-dependent partitioning of  $\text{SO}_2$  is not expected to play an important role in the different sulfate formation observed for  $\text{KNO}_3$  and VL in this

study. The prevailing sulfate formation in VL particles over  $\text{KNO}_3$  particles is likely due to the much lower integrated molar absorptivity of nitrate ( $\sim 143 \text{ M}^{-1} \text{ cm}^{-1}$ ) compared to VL ( $2.8 \times 10^5 \text{ M}^{-1} \text{ cm}^{-1}$ ) over the wavelength range of 300–400 nm (Fig. S1). In addition, this also excluded the possibility of sulfate formation in the gas phase and small nuclei, which would be expected to have condensed/coagulated on both the photosensitizer and  $\text{KNO}_3$  particles. When RH decreased to 20 %, a significant reduction in the average RPAs from 0.26 to 0.002 was observed for VL-coated particles (Fig. S10), attributable to the less dissolved VL for sulfate formation since VL has low solubility and hygroscopicity and the limited  $\text{SO}_2$  dissolution (Liu et al., 2021). In addition, lower RH could result in higher particulate viscosity, which hinders molecular diffusion and reaction (Kroll et al., 2018; González Palacios et al., 2016; Corral Arroyo et al., 2018). A systematic study of the effect of RH on the particle-phase photosensitized reaction is desirable. Overall, sulfate formation was found on VL-coated particles but not on externally mixed nitrate particles at both high and low RH in our study. Oxalic acid is one of the most abundant species of organic aerosols and is commonly found in particles containing atmospheric nitrate (Mochizuki et al., 2017; Cheng et al., 2017; Yang et al., 2009). We have also conducted experiments with internal mixtures of  $\text{KNO}_3$  and oxalic acid, which did not show sulfate formation as well (Fig. 4b). However, internally mixed VL and  $\text{KNO}_3$  yielded 55 % sulfate-containing particles and an average sulfate RPA of 0.12. These values fall in between those of pure  $\text{KNO}_3$  and VL-coated particles (Fig. 4c). As the ion intensity ratio of nitrate to organics of the  $\text{KNO}_3$ –VL internally mixed particles of similar size decreased, higher sulfate RPAs were found. The quantitative sulfate production rate via aerosol-phase  $\text{SO}_2$  oxidation by model photosensitizer is limited by SPAMS measurements in the current study, which focuses on single-particle mixing-state analysis. Further quantitative studies would be useful.

## 4 Environmental implications

This paper presents insights on aerosol  $\text{SO}_2$  oxidation by photosensitizers derived from biomass burning using single-particle characterization. Sulfate formation in photosensitizer-coated particles, in terms of both number percentage and RPA of sulfate, was significantly higher under UV irradiation than under dark conditions. From dark conditions to UV irradiation, the average number percentages of sulfate-containing particles increased from less than 2 % to 43 %–99 %, and the sulfate RPA increased from almost 0 to 0.12–0.67 for SyrAld-, VL- and DMB-coated particles.

The speciation, concentration and properties of photosensitizers in ambient particles are still poorly understood, limiting the parameterization of photosensitized sulfate formation. Nevertheless, we observed that sulfate formation via

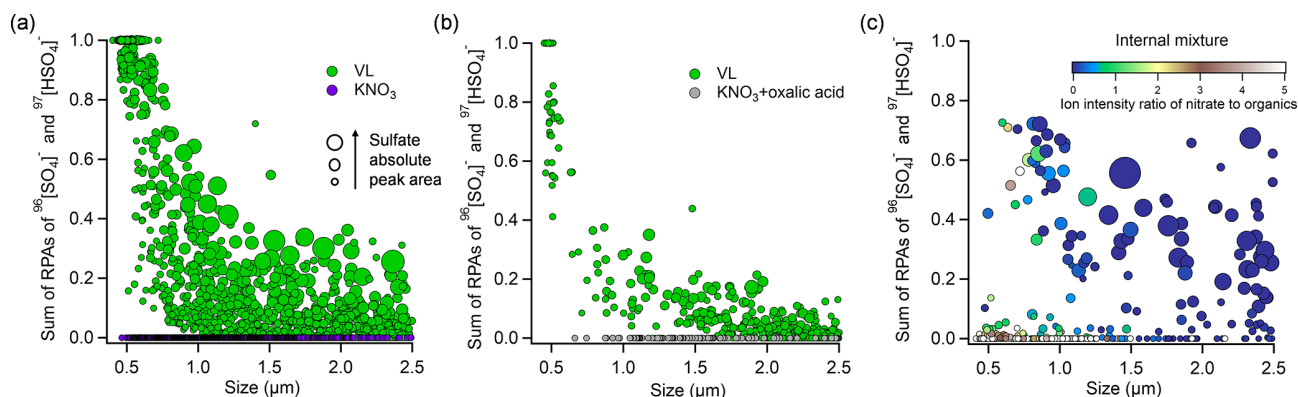


**Figure 4.** Sulfate RPA vs. particle diameter detected by the SPAMS for (a) externally mixed VL-coated particles and  $\text{KNO}_3$ , (b) externally mixed VL-coated particles and  $\text{KNO}_3$ –oxalic acid particles, and (c) internally mixed VL and  $\text{KNO}_3$  particles at 80 % RH under UV irradiation ( $I_1$ ) in the presence of  $\text{SO}_2$ . The markers are presented as a function of sulfate APA. The color scale in (c) indicates the ion intensity ratio of nitrate to organics (total negative ion intensity subtracted by nitrate and sulfate intensity) in the negative mass spectra.

photosensitization is qualitatively more efficient than nitrate photolysis for wet aerosols at 80 % RH. Recently, we found that incense burning particles (considered as typical BBOA surrogates) show increases of sulfate-containing particles and sulfate RPAs by  $\sim 45$  % and  $\sim 0.35$  under UV irradiation than dark conditions, respectively, due to photosensitization reactions of  $\text{SO}_2$  (Liang et al., 2022). These results are within the ranges of our measurements in this paper. The  $\text{SO}_2$  exposure of  $\sim 1800$  ppb min in the OFR in this study corresponds to a 45 and 450 min atmospheric  $\text{SO}_2$  exposure, taking an ambient RH of 80 % and  $\text{SO}_2$  concentration of 40 ppb during extreme haze events (Cheng et al., 2016) and 4 ppb on usual days (Chen et al., 2022), respectively. This indicates that after  $\text{SO}_2$  exposure of tens of minutes to hours, more than 40 % of fresh BBOA particles could contain sulfate via photosensitization, especially under high photon flux such as during typical clear days and haze days in Beijing, China, which were around 4 and 1.4 times, respectively, of that in the OFR ( $I_4$ ) (Fig. S1). Our finding provides additional experimental support to the potentially important contribution of photosensitized oxidation of S(IV) to aerosol sulfate formation in biomass burning plumes. Future studies of the quantification and mechanism revelation of sulfate formation via photosensitization are needed. In addition, we solely studied three typical photosensitizers derived from biomass burning. Photosensitized sulfate formation on real BBOA particles, which is a complex matrix of organics, is to be explored further.

**Data availability.** The data are available upon request to the corresponding authors.

**Supplement.** The supplement related to this article is available online at: <https://doi.org/10.5194/acp-23-5251-2023-supplement>.

**Author contributions.** CKC and LZ designed the experiment; LZ and ZL conducted the experiments; LZ and ZL performed the data interpretation; LZ, ZL, BRG, RAIC, RT, ML, CC, and CKC wrote the paper. All authors contributed to the paper with useful scientific discussions or comments.

**Competing interests.** The contact author has declared that none of the authors has any competing interests.

**Disclaimer.** Publisher's note: Copernicus Publications remains neutral with regard to jurisdictional claims in published maps and institutional affiliations.

**Acknowledgements.** We gratefully acknowledge the support from the Hong Kong Research Grants Council (grant nos. 11304121, 11314222, and R1016-20F) and the National Natural Science Foundation of China (grant no. 42275104).

**Financial support.** This research has been supported by the Hong Kong Research Grants Council (grant nos. 11304121, 11314222, and R1016-20F) and the National Natural Science Foundation of China (grant no. 42275104).

**Review statement.** This paper was edited by Ryan Sullivan and reviewed by three anonymous referees.

## References

Alexander, B., Park, R. J., Jacob, D. J., and Gong, S.: Transition metal-catalyzed oxidation of atmospheric sulfur: Global implications for the sulfur budget, *J. Geophys. Res.-Atmos.*, 114, D02309, <https://doi.org/10.101029/02008jd010486>, 2009.



- Anastasio, C., Faust, B. C., and Rao, C. J.: Aromatic carbonyl compounds as aqueous-phase photochemical sources of hydrogen peroxide in acidic sulfate aerosols, fogs, and clouds. 1. Non-phenolic methoxybenzaldehydes and methoxyacetophenones with reductants (phenols), *Environ. Sci. Technol.*, 31, 218–232, 1996.
- Calvert, J. G., Su, F., Bottenheim, J. W., and Strausz, O. P.: Mechanism of the homogeneous oxidation of sulfur dioxide in the troposphere, *Atmos. Environ.*, 12, 197–226, [https://doi.org/10.1016/0004-6981\(78\)90201-9](https://doi.org/10.1016/0004-6981(78)90201-9), 1978.
- Canonica, S., Jans, U., Stemmler, K., and Hoigne, J.: Transformation kinetics of phenols in water: photosensitization by dissolved natural organic material and aromatic ketones, *Environ. Sci. Technol.*, 29, 1822–1831, 1995.
- Chan, C. K. and Yao, X.: Air pollution in mega cities in China, *Atmos. Environ.*, 42, 1–42, 2008.
- Chen, C.-H., Tsai, C.-Y., Chen, T.-F., Hou, L.-S., and Chang, K.-H.: Temporal Trends and Spatial Distribution Characteristics of Air Quality Monitored in China from 2015 to 2020, *Journal of Innovative Technology*, 4, 23–28, 2022.
- Chen, Y., Li, N., Li, X., Tao, Y., Luo, S., Zhao, Z., Ma, S., Huang, H., Chen, Y., and Ye, Z.: Secondary organic aerosol formation from 3C\*-initiated oxidation of 4-ethylguaiaicol in atmospheric aqueous-phase, *Sci. Total Environ.*, 723, 137953, <https://doi.org/10.1016/j.scitotenv.2020.137953>, 2020.
- Cheng, C., Li, M., Chan, C. K., Tong, H., Chen, C., Chen, D., Wu, D., Li, L., Wu, C., Cheng, P., Gao, W., Huang, Z., Li, X., Zhang, Z., Fu, Z., Bi, Y., and Zhou, Z.: Mixing state of oxalic acid containing particles in the rural area of Pearl River Delta, China: implications for the formation mechanism of oxalic acid, *Atmos. Chem. Phys.*, 17, 9519–9533, <https://doi.org/10.5194/acp-17-9519-2017>, 2017.
- Cheng, Y., Zheng, G., Wei, C., Mu, Q., Zheng, B., Wang, Z., Gao, M., Zhang, Q., He, K., and Carmichael, G.: Reactive nitrogen chemistry in aerosol water as a source of sulfate during haze events in China, *Sci. Adv.*, 2, e1601530, <https://doi.org/10.1126/sciadv.1601530>, 2016.
- Corral Arroyo, P., Bartels-Rausch, T., Alpert, P. A., Dumas, S. P., Perrier, S. B., George, C., and Ammann, M.: Particle-phase photosensitized radical production and aerosol aging, *Environ. Sci. Technol.*, 52, 7680–7688, 2018.
- Dalrymple, R. M., Carfagno, A. K., and Sharpless, C. M.: Correlations between dissolved organic matter optical properties and quantum yields of singlet oxygen and hydrogen peroxide, *Environ. Sci. Technol.*, 44, 5824–5829, 2010.
- Felber, T., Schaefer, T., He, L., and Herrmann, H.: Aromatic Carbonyl and Nitro Compounds as Photosensitizers and Their Photophysical Properties in the Tropospheric Aqueous Phase, *J. Phys. Chem. A*, 125, 5078–5095, 2021.
- Freney, E. J., Martin, S. T., and Buseck, P. R.: Deliquescence and efflorescence of potassium salts relevant to biomass-burning aerosol particles, *Aerosol Sci. Technol.*, 43, 799–807, 2009.
- Fuzzi, S., Baltensperger, U., Carslaw, K., Decesari, S., Denier van der Gon, H., Facchini, M. C., Fowler, D., Koren, I., Langford, B., Lohmann, U., Nemitz, E., Pandis, S., Riipinen, I., Rudich, Y., Schaap, M., Slowik, J. G., Spracklen, D. V., Vignati, E., Wild, M., Williams, M., and Gilardoni, S.: Particulate matter, air quality and climate: lessons learned and future needs, *Atmos. Chem. Phys.*, 15, 8217–8299, <https://doi.org/10.5194/acp-15-8217-2015>, 2015.
- Gen, M., Zhang, R., Huang, D. D., Li, Y., and Chan, C. K.: Heterogeneous SO<sub>2</sub> oxidation in sulfate formation by photolysis of particulate nitrate, *Environ. Sci. Technol. Lett.*, 6, 86–91, 2019a.
- Gen, M., Zhang, R., Huang, D. D., Li, Y., and Chan, C. K.: Heterogeneous oxidation of SO<sub>2</sub> in sulfate production during nitrate photolysis at 300 nm: effect of pH, relative humidity, irradiation intensity, and the presence of organic compounds, *Environ. Sci. Technol.*, 53, 8757–8766, 2019b.
- Gen, M., Liang, Z., Zhang, R., Go Mabato, B. R., and Chan, C. K.: Particulate nitrate photolysis in the atmosphere, *Environ. Sci. Atmos.*, 2, 111–127, <https://doi.org/10.1039/d1ea00087j>, 2022.
- George, C., Ammann, M., D'Anna, B., Donaldson, D., and Nizkorodov, S. A.: Heterogeneous photochemistry in the atmosphere, *Chem. Rev.*, 115, 4218–4258, 2015.
- George, C., Brüggemann, M., Hayeck, N., Tinel, L., and Donaldson, J.: Interfacial photochemistry: physical chemistry of gas-liquid interfaces, in: *Developments in Physical & Theoretical Chemistry*, edited by: Faust, J. A. and House, J. E., Elsevier, 435–457, <https://doi.org/10.1016/B978-0-12-813641-6.00014-5>, 2018.
- Gomez Alvarez, E., Wortham, H., Streckowski, R., Zetzsch, C., and Gligorovski, S.: Atmospheric photosensitized heterogeneous and multiphase reactions: from outdoors to indoors, *Environ. Sci. Technol.*, 46, 1955–1963, <https://doi.org/10.1021/es2019675>, 2012.
- González Palacios, L., Corral Arroyo, P., Aregahegn, K. Z., Steimer, S. S., Bartels-Rausch, T., Nozière, B., George, C., Ammann, M., and Volkamer, R.: Heterogeneous photochemistry of imidazole-2-carboxaldehyde: HO<sub>2</sub> radical formation and aerosol growth, *Atmos. Chem. Phys.*, 16, 11823–11836, <https://doi.org/10.5194/acp-16-11823-2016>, 2016.
- Grantz, D., Garner, J., and Johnson, D.: Ecological effects of particulate matter, *Environ. Int.*, 29, 213–239, 2003.
- Gross, D. S., Galli, M. E., Silva, P. J., and Prather, K. A.: Relative sensitivity factors for alkali metal and ammonium cations in single-particle aerosol time-of-flight mass spectra, *Anal. Chem.*, 72, 416–422, 2000.
- Guazzotti, S. A., Coffee, K. R., and Prather, K. A.: Continuous measurements of size-resolved particle chemistry during INDOEX-Intensive Field Phase 99, *J. Geophys. Res.-Atmos.*, 106, 28607–28627, 2001.
- Harris, E., Sinha, B., Van Pinxteren, D., Tilgner, A., Fomba, K. W., Schneider, J., Roth, A., Gnauk, T., Fahlbusch, B., and Mertes, S.: Enhanced role of transition metal ion catalysis during in-cloud oxidation of SO<sub>2</sub>, *Science*, 340, 727–730, 2013.
- Hatch, L. E., Pratt, K. A., Huffman, J. A., Jimenez, J. L., and Prather, K. A.: Impacts of aerosol aging on laser desorption/ionization in single-particle mass spectrometers, *Aerosol Sci. Technol.*, 48, 1050–1058, 2014.
- Hoffmann, M. R. and Calvert, J. G.: Chemical Transformation Modules for Eulerian Acid Deposition Models: Volume II, the Aqueous-phase Chemistry, EPA/600/3-85, 17, 1985.
- Hu, X., Guo, Z., Sun, W., Lian, X., Fu, Y., Meng, H., Zhu, Y., Zhang, G., Wang, X., and Xue, L.: Atmospheric Processing of Particulate Imidazole Compounds Driven by Photochemistry, *Environ. Sci. Technol. Lett.*, 9, 265–271, 2022.
- Hudda, N. and Fruin, S.: International airport impacts to air quality: size and related properties of large increases in ultrafine particle

- number concentrations, *Environ. Sci. Technol.*, 50, 3362–3370, 2016.
- Hussain, K., Thorsen, G., and Malthe-Sørensen, D.: Nucleation and metastability in crystallization of vanillin and ethyl vanillin, *Chem. Eng. Sci.*, 56, 2295–2304, 2001.
- Ibusuki, T. and Takeuchi, K.: Sulfur dioxide oxidation by oxygen catalyzed by mixtures of manganese (II) and iron (III) in aqueous solutions at environmental reaction conditions, *Atmos. Environ.*, 21, 1555–1560, 1987.
- Jahn, L. G., Jahl, L. G., Bowers, B. B., and Sullivan, R. C.: Morphology of organic carbon coatings on biomass-burning particles and their role in reactive gas uptake, *ACS Earth Space Chem.*, 5, 2184–2195, 2021.
- Kaur, R. and Anastasio, C.: First measurements of organic triplet excited states in atmospheric waters, *Environ. Sci. Technol.*, 52, 5218–5226, 2018.
- Kaur, R., Labins, J. R., Helbock, S. S., Jiang, W., Bein, K. J., Zhang, Q., and Anastasio, C.: Photooxidants from brown carbon and other chromophores in illuminated particle extracts, *Atmos. Chem. Phys.*, 19, 6579–6594, <https://doi.org/10.5194/acp-19-6579-2019>, 2019.
- Kavuru, P., Grebinoski, S. J., Patel, M. A., Wojtas, L., and Chadwick, K.: Polymorphism of vanillin revisited: the discovery and selective crystallization of a rare crystal structure, *CrystEng-Comm*, 18, 1118–1122, 2016.
- Kroll, J. A., Frandsen, B. N., Kjaergaard, H. G., and Vaida, V.: Atmospheric hydroxyl radical source: Reaction of triplet SO<sub>2</sub> and water, *J. Phys. Chem. A*, 122, 4465–4469, 2018.
- Li, L., Huang, Z., Dong, J., Li, M., Gao, W., Nian, H., Fu, Z., Zhang, G., Bi, X., and Cheng, P.: Real time bipolar time-of-flight mass spectrometer for analyzing single aerosol particles, *Int. J. Mass Spectrom.*, 303, 118–124, 2011.
- Li, Y. J., Yeung, J. W., Leung, T. P., Lau, A. P., and Chan, C. K.: Characterization of organic particles from incense burning using an aerodyne high-resolution time-of-flight aerosol mass spectrometer, *Aerosol Sci. Technol.*, 46, 654–665, 2012.
- Liang, Z., Zhou, L., Infante Cuevas, R. A., Li, X., Cheng, C., Li, M., Tang, R., Zhang, R., Lee, P. K., and Lai, A. C.: Sulfate Formation in Incense Burning Particles: A Single-Particle Mass Spectrometric Study, *Environ. Sci. Technol. Lett.*, 9, 718–725 <https://doi.org/10.1021/acs.estlett.2c00492>, 2022.
- Liu, T. and Abbatt, J. P.: An experimental assessment of the importance of S (IV) oxidation by hypohalous acids in the marine atmosphere, *Geophys. Res. Lett.*, 47, e2019GL086465, <https://doi.org/10.1029/2019GL086465>, 2020.
- Liu, T. and Abbatt, J. P.: Oxidation of sulfur dioxide by nitrogen dioxide accelerated at the interface of deliquesced aerosol particles, *Nature Chem.* 13, 1173–1177, 2021.
- Liu, T., Clegg, S. L., and Abbatt, J. P.: Fast oxidation of sulfur dioxide by hydrogen peroxide in deliquesced aerosol particles, *P. Natl. Acad. Sci. USA*, 117, 1354–1359, 2020.
- Liu, T., Chan, A. W., and Abbatt, J. P.: Multiphase oxidation of sulfur dioxide in aerosol particles: implications for sulfate formation in polluted environments, *Environ. Sci. Technol.*, 55, 4227–4242, 2021.
- Liu, W. and Sun, S.: Ultrastructural changes of tracheal epithelium and alveolar macrophages of rats exposed to mosquito coil smoke, *Toxicol. Lett.*, 41, 145–157, 1988.
- Mabato, B. R. G., Lyu, Y., Ji, Y., Li, Y. J., Huang, D. D., Li, X., Nah, T., Lam, C. H., and Chan, C. K.: Aqueous secondary organic aerosol formation from the direct photosensitized oxidation of vanillin in the absence and presence of ammonium nitrate, *Atmos. Chem. Phys.*, 22, 273–293, <https://doi.org/10.5194/acp-22-273-2022>, 2022.
- Mabato, B. R. G., Li, Y. J., Huang, D. D., Wang, Y., and Chan, C. K.: Comparison of aqueous secondary organic aerosol (aq-SOA) product distributions from guaiacol oxidation by non-phenolic and phenolic methoxybenzaldehydes as photosensitizers in the absence and presence of ammonium nitrate, *Atmos. Chem. Phys.*, 23, 2859–2875, <https://doi.org/10.5194/acp-23-2859-2023>, 2023.
- Martin, L. R. and Good, T. W.: Catalyzed oxidation of sulfur dioxide in solution: The iron-manganese synergism, *Atmos. Environ. A.*, 25, 2395–2399, 1991.
- Martins-Costa, M. T., Anglada, J. M., Francisco, J. S., and Ruiz-López, M. F.: Photochemistry of SO<sub>2</sub> at the air–water interface: a source of OH and HOSO radicals, *J. Am. Chem. Soc.*, 140, 12341–12344, 2018.
- Mochida, M. and Kawamura, K.: Hygroscopic properties of levoglucosan and related organic compounds characteristic to biomass burning aerosol particles, *J. Geophys. Res.-Atmos.*, 109, D21202, <https://doi.org/10.1029/2004JD004962>, 2004.
- Mochizuki, T., Kawamura, K., Miyazaki, Y., Wada, R., Takahashi, Y., Saigusa, N., and Tani, A.: Secondary formation of oxalic acid and related organic species from biogenic sources in a larch forest at the northern slope of Mt. Fuji, *Atmos. Environ.*, 166, 255–262, 2017.
- Nel, A.: Air pollution-related illness: effects of particles, *Science*, 308, 804–806, 2005.
- Neubauer, K. R., Johnston, M. V., and Wexler, A. S.: Humidity effects on the mass spectra of single aerosol particles, *Atmos. Environ.*, 32, 2521–2529, 1998.
- Nolte, C. G., Schauer, J. J., Cass, G. R., and Simoneit, B. R.: Highly polar organic compounds present in wood smoke and in the ambient atmosphere, *Environ. Sci. Technol.*, 35, 1912–1919, 2001.
- Peng, D.-Q., Yu, Z.-X., Wang, C.-H., Gong, B., Liu, Y.-Y., and Wei, J.-H.: Chemical Constituents and Anti-Inflammatory Effect of Incense Smoke from Agarwood Determined by GC-MS, *Int. J. Anal. Chem.*, 2020, 4575030, <https://doi.org/10.1155/2020/4575030>, 2020.
- Pratt, K. A., Mayer, J. E., Holecek, J. C., Moffet, R. C., Sanchez, R. O., Rebotier, T. P., Furutani, H., Gonin, M., Fuhrer, K., and Su, Y.: Development and characterization of an aircraft aerosol time-of-flight mass spectrometer, *Anal. Chem.*, 81, 1792–1800, 2009.
- Qi, C., Stanley, N., Pui, D. Y., and Kuehn, T. H.: Laboratory and on-road evaluations of cabin air filters using number and surface area concentration monitors, *Environ. Sci. Technol.*, 42, 4128–4132, 2008.
- Qi, X., Pang, X., Hong, Y., Wang, Y., Lou, S., Feng, J., Cheng, P., and Zhou, Z.: Real-time analysis of the homogeneous and heterogeneous reactions of pyrene with ozone by SPAMS and CRD-EAS, *Chemosphere*, 234, 608–617, 2019.
- Reinard, M. S. and Johnston, M. V.: Ion formation mechanism in laser desorption ionization of individual nanoparticles, *J. Am. Soc. Mass Spectrom.*, 19, 389–399, 2008.

- Rogge, W. F., Hildemann, L. M., Mazurek, M. A., Cass, G. R., and Simoneit, B. R.: Sources of fine organic aerosol. 9. Pine, oak, and synthetic log combustion in residential fireplaces, *Environ. Sci. Technol.*, 32, 13–22, 1998.
- Rubasinghege, G. and Grassian, V. H.: Role (s) of adsorbed water in the surface chemistry of environmental interfaces, *Chem. Commun.*, 49, 3071–3094, 2013.
- Schauer, J. J., Kleeman, M. J., Cass, G. R., and Simoneit, B. R.: Measurement of emissions from air pollution sources. 3. C1–C29 organic compounds from fireplace combustion of wood, *Environ. Sci. Technol.*, 35, 1716–1728, 2001.
- Simoneit, B. R., Rogge, W., Mazurek, M., Standley, L., Hildemann, L., and Cass, G.: Lignin pyrolysis products, lignans, and resin acids as specific tracers of plant classes in emissions from biomass combustion, *Environ. Sci. Technol.*, 27, 2533–2541, 1993.
- Smith, J. D., Sio, V., Yu, L., Zhang, Q., and Anastasio, C.: Secondary organic aerosol production from aqueous reactions of atmospheric phenols with an organic triplet excited state, *Environ. Sci. Technol.*, 48, 1049–1057, 2014.
- Smith, J. D., Kinney, H., and Anastasio, C.: Aqueous benzene-diols react with an organic triplet excited state and hydroxyl radical to form secondary organic aerosol, *Phys. Chem. Chem. Phys.*, 17, 10227–10237, 2015.
- Smith, J. D., Kinney, H., and Anastasio, C.: Phenolic carbonyls undergo rapid aqueous photodegradation to form low-volatility, light-absorbing products, *Atmos. Environ.*, 126, 36–44, 2016.
- Walcek, C. J. and Taylor, G. R.: A theoretical method for computing vertical distributions of acidity and sulfate production within cumulus clouds, *J. Atmos. Sci.*, 43, 339–355, 1986.
- Wang, G., Zhang, R., Gomez, M. E., Yang, L., Levy Zamora, M., Hu, M., Lin, Y., Peng, J., Guo, S., and Meng, J.: Persistent sulfate formation from London Fog to Chinese haze, *P. Natl. Acad. Sci. USA*, 113, 13630–13635, 2016.
- Wang, X., Gemayel, R., Hayeck, N., Perrier, S., Charbonnel, N., Xu, C., Chen, H., Zhu, C., Zhang, L., and Wang, L.: Atmospheric photosensitization: a new pathway for sulfate formation, *Environ. Sci. Technol.*, 54, 3114–3120, 2020.
- Wang, X., Gemayel, R., Baboian, V. J., Li, K., Boreave, A., Dubois, C., Tomaz, S., Perrier, S., Nizkorodov, S. A., and George, C.: Naphthalene-Derived Secondary Organic Aerosols Interfacial Photosensitizing Properties, *Geophys. Res. Lett.*, 48, e2021GL093465, <https://doi.org/10.1029/2021GL093465>, 2021.
- Wang, Y., Zhang, Q., Jiang, J., Zhou, W., Wang, B., He, K., Duan, F., Zhang, Q., Philip, S., and Xie, Y.: Enhanced sulfate formation during China's severe winter haze episode in January 2013 missing from current models, *J. Geophys. Res.-Atmos.*, 119, 10425–10440, <https://doi.org/10.1002/2013JD021426>, 2014.
- Willeke, K. and Whitby, K. T.: Atmospheric aerosols: size distribution interpretation, *J. Air Pollut. Control A.*, 25, 529–534, 1975.
- Yang, F., Chen, H., Wang, X., Yang, X., Du, J., and Chen, J.: Single particle mass spectrometry of oxalic acid in ambient aerosols in Shanghai: Mixing state and formation mechanism, *Atmos. Environ.*, 43, 3876–3882, 2009.
- Yao, M., Zhao, Y., Hu, M., Huang, D., Wang, Y., Yu, J. Z., and Yan, N.: Multiphase reactions between secondary organic aerosol and sulfur dioxide: kinetics and contributions to sulfate formation and aerosol aging, *Environ. Sci. Technol. Lett.*, 6, 768–774, 2019.
- Ye, J., Abbatt, J. P. D., and Chan, A. W. H.: Novel pathway of SO<sub>2</sub> oxidation in the atmosphere: reactions with monoterpene ozonolysis intermediates and secondary organic aerosol, *Atmos. Chem. Phys.*, 18, 5549–5565, <https://doi.org/10.5194/acp-18-5549-2018>, 2018.
- Zauscher, M. D., Wang, Y., Moore, M. J., Gaston, C. J., and Prather, K. A.: Air quality impact and physicochemical aging of biomass burning aerosols during the 2007 San Diego wildfires, *Environ. Sci. Technol.*, 47, 7633–7643, 2013.
- Zhang, R., Wang, G., Guo, S., Zamora, M. L., Ying, Q., Lin, Y., Wang, W., Hu, M., and Wang, Y.: Formation of urban fine particulate matter, *Chem. Rev.*, 115, 3803–3855, 2015.
- Zhang, R., Gen, M., Huang, D., Li, Y., and Chan, C. K.: Enhanced sulfate production by nitrate photolysis in the presence of halide ions in atmospheric particles, *Environ. Sci. Technol.*, 54, 3831–3839, 2020.
- Zhang, Y., Li, W., Li, L., Li, M., Zhou, Z., Yu, J., and Zhou, Y.: Source apportionment of PM<sub>2.5</sub> using PMF combined on-line bulk and single-particle measurements: Contribution of fireworks and biomass burning, *J. Environ. Sci.*, 136, 325–336, <https://doi.org/10.1016/j.jes.2022.12.019>, 2022.
- Zhang, Y. M., Zhang, X. Y., Sun, J. Y., Hu, G. Y., Shen, X. J., Wang, Y. Q., Wang, T. T., Wang, D. Z., and Zhao, Y.: Chemical composition and mass size distribution of PM<sub>1</sub> at an elevated site in central east China, *Atmos. Chem. Phys.*, 14, 12237–12249, <https://doi.org/10.5194/acp-14-12237-2014>, 2014.
- Zheng, B., Zhang, Q., Zhang, Y., He, K. B., Wang, K., Zheng, G. J., Duan, F. K., Ma, Y. L., and Kimoto, T.: Heterogeneous chemistry: a mechanism missing in current models to explain secondary inorganic aerosol formation during the January 2013 haze episode in North China, *Atmos. Chem. Phys.*, 15, 2031–2049, <https://doi.org/10.5194/acp-15-2031-2015>, 2015.
- Zhou, L., Li, M., Cheng, C., Zhou, Z., Nian, H., Tang, R., and Chan, C. K.: Real-time chemical characterization of single ambient particles at a port city in Chinese domestic emission control area – Impacts of ship emissions on urban air quality, *Sci. Total Environ.*, 819, 153117, <https://doi.org/10.1016/j.scitotenv.2022.153117>, 2022.
- Zhou, Y., Huang, X. H., Griffith, S. M., Li, M., Li, L., Zhou, Z., Wu, C., Meng, J., Chan, C. K., and Louie, P. K.: A field measurement based scaling approach for quantification of major ions, organic carbon, and elemental carbon using a single particle aerosol mass spectrometer, *Atmos. Environ.*, 143, 300–312, 2016.
- Zuend, A., Marcolli, C., Luo, B. P., and Peter, T.: A thermodynamic model of mixed organic-inorganic aerosols to predict activity coefficients, *Atmos. Chem. Phys.*, 8, 4559–4593, <https://doi.org/10.5194/acp-8-4559-2008>, 2008.